

X-ray resonant Raman scattering at the Kr K-edge

T. LeBrun, S.H. Southworth, R.W. Dunford, D.S. Gemmell, S. Hasegawa, E.P. Kanter, B. Krässig, and L. Young
Argonne National Laboratory, Argonne, IL 60439 USA

Introduction

When an atomic inner-shell vacancy is produced by particle impact or photoionization far above threshold, the resulting x-ray fluorescence spectrum (XFS) has characteristic energies, intensities, and line shapes. A two-step model, in which the vacancy creation process and the radiative decay process are treated independently, is adequate to describe the XFS. However, when vacancies are produced by photoabsorption at energies near resonances or the ionization threshold, the XFS is modified and is sensitive to the precise energy and bandwidth of the incident x-ray beam. In that case, the vacancy excitation and decay steps are coupled and described as a one-step, resonant inelastic scattering process referred to as x-ray resonant Raman scattering (XRRS) [1]. We have used an x-ray emission spectrometer on the BESSRC-CAT undulator beamline (12-ID) to study XRRS in the Kr $K\alpha_{1,2}$ x-ray emission spectrum by tuning the incident x-ray energy through the K-edge at 14326 eV.

X-ray emission spectrometer

A diagram of the x-ray spectrometer is shown in Figure 1. The x-ray beam from the undulator beamline's Si(111) double-crystal monochromator passed through a gas cell containing 1 atmosphere of Kr. Ion chambers at the front and back of the Kr cell measured the incident and transmitted x-ray fluxes. The incident x-ray beam produces a line-like source of emitted x-rays in the Kr cell, and the spectrometer was optimized for this geometry. A 5–10 mm line of emitted x-rays was collimated with apertures, dispersed with two flat Si(111) crystals oriented in high-resolution dispersive geometry, and recorded by a NaI scintillation detector.

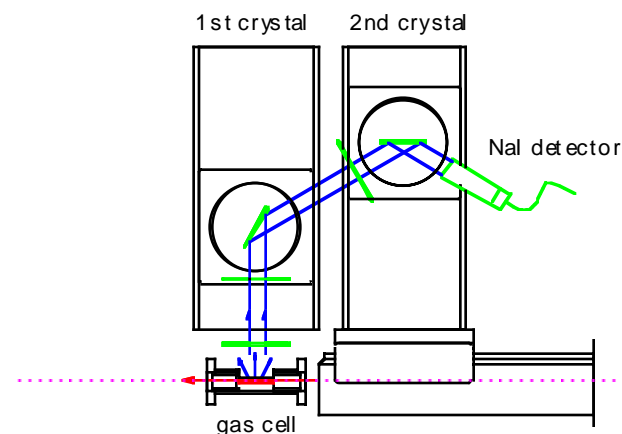


Figure 1: Diagram of x-ray emission spectrometer.

The crystals were oriented on precision translational and rotary stages under computer control to allow more complex experimental geometries in the future, including curved-

crystal scans along the Rowland circle. In the present geometry, x-ray spectra were recorded by step scanning the first crystal with the second crystal fixed. This varied the Bragg angle defined by the two-crystal system at half the angular speed as the included angle. A double-flat-crystal system was chosen for initial experiments to allow the resolution to approach the theoretical limit for Si(111), $\Delta E/E = 1.41 \times 10^{-4}$.

The Kr $K\alpha_{1,2}$ XFS excited 84 eV above the K-edge is shown in Figure 2. The two-step model is adequate at this excitation energy, and we observe the characteristic fluorescence spectrum. The measured peak widths of 5.3 eV was dominated by the 4 eV natural width and indicates an instrumental resolution of 2.4 eV, which is 33% higher than the intrinsic resolution of Si(111) at this energy.

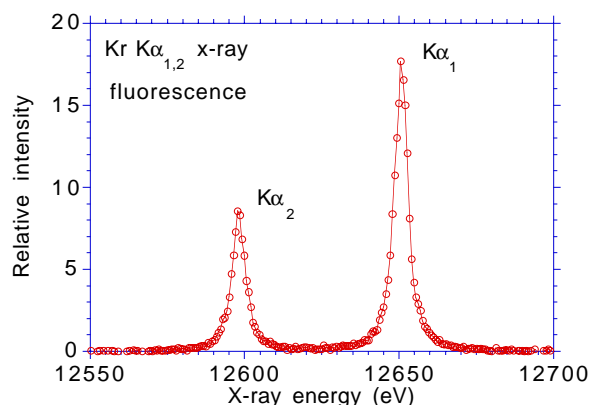


Figure 2: Kr $K\alpha_{1,2}$ fluorescence spectrum.

Resonant Raman scattering

The Kr $1s \rightarrow np$, $n = 5, 6, 7, \dots$ pre-edge Rydberg structure is washed out by lifetime broadening in the K-edge absorption spectrum [2]. However, using the XRRS process, high-resolution x-ray emission measurements can be sensitive to resonance and threshold structure at effectively higher resolution than absorption spectra [3]. XRRS-based measurements should be interpreted with some caution because in principle, the final state cross sections are sensitive to many-electron effects and intermediate-state interference [1, 4]. Those complications will be ignored in this brief report. Figure 3 shows a set of Kr $K\alpha_{1,2}$ x-ray emission spectra recorded at excitation energies across the K-edge. Comparison with the characteristic fluorescence spectrum in Figure 2 shows that asymmetric line shapes are observed below the edge. This effect results from energy conservation (i.e., there is insufficient energy to fully develop the fluorescence peak) [5].

Using Si(111) crystals, the bandwidths of the incident x-ray beam (≈ 4.7 eV) and of the emission spectrometer (≈ 2.4 eV) were too large to resolve bound final states (e.g., $[2p]5p$, in the emission spectra of Figure 3).

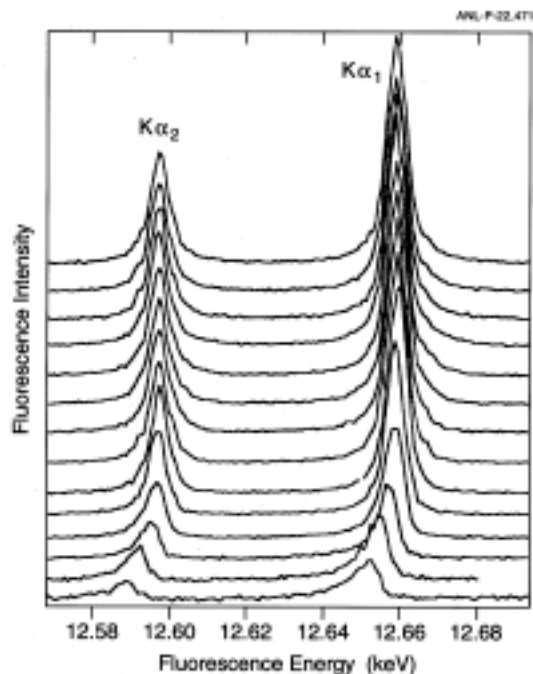


Figure 3: Variation of Kr $K\alpha_{1,2}$ x-ray emission across the K-edge.

However, the method of Hämäläinen *et al.* [3] was used to explore resonance and threshold effects by comparing the high-resolution x-ray fluorescence yield (HRXY) with the total absorption cross section. The HRXY is defined here as the relative intensity of emitted x-rays in the spectrometer bandwidth centered on the $K\alpha_1$ characteristic peak and is plotted in Figure 4 in comparison with the total photoabsorption cross section.

In Figure 4, the HRXY has a sharper onset and intensity spike in the resonance and threshold region than does the absorption cross section. In addition, at ≈ 30 eV above threshold, the HRXY appears to be insensitive to multielectron excitation features in the absorption spectrum [2]. Multielectron excitations give rise to satellite peaks in x-ray emission, which presumably are excluded from the fluorescence yield measured here at the $K\alpha_1$ peak energy. We conclude that by selecting a narrow band of final states, the HRXY gives information on resonance and threshold structure, which complements total absorption cross section studies. More detailed information on atomic XRRS will result from future studies using higher resolution of both the incident and emitted x-rays.

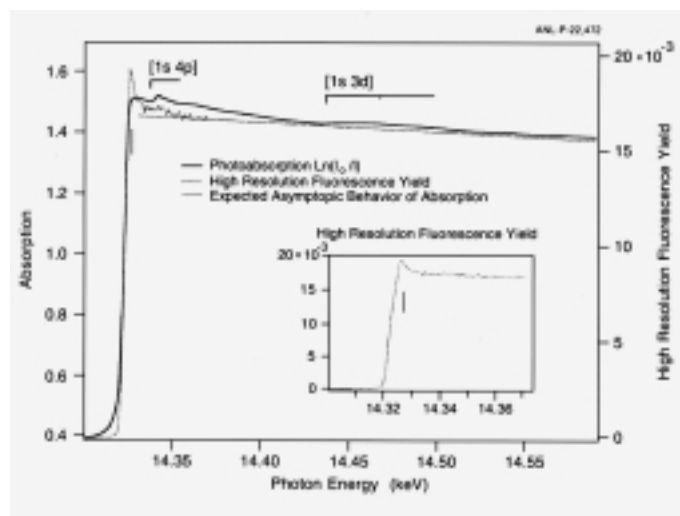


Figure 4: Comparison of Kr $K\alpha_1$ high-resolution fluorescence yield (dotted line) with the total photoabsorption cross section (thick solid line). The thin solid line shows the expected $E^{-7/2}$ asymptotic dependence on x-ray energy of the Kr 1s photoionization cross section, normalized to the high-resolution fluorescence yield. Structures in the absorption cross section due to $[1s4p]$ and $[1s3d]$ multielectron excitations are indicated [2].

Acknowledgments

We thank B. Zabransky for major contributions to the design and assembly of the x-ray spectrometer, and we thank the BESSRC staff for their support in beamline operations. This work was supported by the U.S. Department of Energy, Office of Basic Energy Sciences, Division of Chemical Sciences, under Contract No. W-31-109-Eng-38. Use of the Advanced Photon Source was supported by the U.S. Department of Energy, Basic Energy Sciences, Office of Science, under Contract No. W-31-109-Eng-38.

References

- [1] T. Åberg and B. Crasemann, in *Resonant Anomalous X-Ray Scattering: Theory and Applications*, ed. G. Materlik, C.J. Sparks, and K. Fischer (North-Holland, Amsterdam, 1994), 431.
- [2] S.J. Schaphorst, A.F. Kodre, J. Ruschinski, B. Crasemann, T. Åberg, J. Tulkki, M.H. Chen, Y. Azuma, and G.S. Brown, *Phys. Rev. A* **47**, 1953 (1993).
- [3] K. Hämäläinen, D.P. Siddons, J.B. Hastings, and L.E. Berman, *Phys. Rev. Lett.* **67**, 2850 (1991).
- [4] P. Carra, M. Fabrizio, and B. T. Thole, *Phys. Rev. Lett.* **74**, 3700 (1995).
- [5] J. Tulkki, *Phys. Rev. A* **27**, 3375 (1983).